The Astrophysical Journal, 613:1221–1232, 2004 October 1

EXTERNAL AND INTERNAL RECONNECTION IN TWO FILAMENT-CARRYING MAGNETIC CAVITY SOLAR ERUPTIONS

Alphonse C. Sterling and Ronald L. Moore
NASA Marshall Space Flight Center, SD50/Space Science Department, Huntsville, AL 35812;
asterling@solar.stanford.edu, ron.moore@nasa.gov
Received 2004 February 21; accepted 2004 June 11

ABSTRACT

We observe two near-limb solar filament eruptions, one of 2000 February 26 and the other of 2002 January 4. For both we use 195 Å Fe xii images from the Extreme-Ultraviolet Imaging Telescope (EIT) and magnetograms from the Michelson Doppler Imager (MDI), both of which are on the *Solar and Heliospheric Observatory* (*SOHO*). For the earlier event we also use soft X-ray telescope (SXT), hard X-ray telescope (HXT), and Bragg Crystal Spectrometer (BCS) data from the *Yohkoh* satellite, and hard X-ray data from the BATSE experiment on the *Compton Gamma Ray Observatory* (*CGRO*). Both events occur in quadrupolar magnetic regions, and both have coronal features that we infer belong to the same magnetic cavity structures as the filaments. In both cases, the cavity and filament first rise slowly at $\sim$10 km s^{-1} prior to eruption and then accelerate to $\sim$100 km s^{-1} during the eruption, although the slow-rise movement for the higher altitude cavity elements is clearer in the later event. We estimate that both filaments and both cavities contain masses of $\sim 10^{14}$–10^{15} and $\sim 10^{15}$–10^{16} g, respectively. We consider whether two specific magnetic reconnection–based models for eruption onset, the "tether cutting" and the "breakout" models, are consistent with our observations. In the earlier event, soft X-rays from SXT show an intensity increase during the 12 minute interval over which fast eruption begins, which is consistent with tether-cutting–model predictions. Substantial hard X-rays, however, do not occur until after fast eruption is underway, and so this is a constraint the tether-cutting model must satisfy. During the same 12 minute interval over which fast eruption begins, there are brightenings and topological changes in the corona indicative of high-altitude reconnection early in the eruption, and this is consistent with breakout predictions. In both eruptions, the state of the overlying loops at the time of onset of the fast-rise phase of the corresponding filament can be compared with expectations from the breakout model, thereby setting constraints that the breakout model must meet. Our findings are consistent with both runaway tether-cutting–type reconnection and fast breakout-type reconnection, occurring early in the fast phase of the February eruption and with both types of reconnection being important in unleashing the explosion, but we are not able to say which, if either, type of reconnection actually triggered the fast phase. In any case, we have found specific constraints that either model, or any other model, must satisfy if correct.

Subject headings: Sun: corona — Sun: coronal mass ejections (CMEs) — Sun: flares — Sun: magnetic fields — Sun: UV radiation

Online material: color figure

1. INTRODUCTION

Not all solar eruptions include easily observable ejective filaments, but for those that do the filament (or prominence) material can be a useful tracer of low coronal magnetic field lines that might otherwise be difficult to observe. Filaments, however, only occupy a limited volume of a more general erupting magnetic structure, which sometimes takes the form of a magnetic cavity (e.g., Gopalswamy & Hanaoka 1998; Hudson et al. 1999). After eruption, such magnetic cavities sometimes appear in white light observations of coronal mass ejections (CMEs), which often show a three-part structure, with the expelled filament material preceded by a cavity-like nearly transparent middle region and a bright outer edge. Recently we have been investigating the solar eruption mechanism through observations of events involving filament or prominence ejections (Sterling & Moore 2003, 2004). Here we extend these investigations to two magnetic cavity eruptions. For each case, we see a near-limb filament and associated higher coronal features, all of which we infer belong to or are contiguous with a common magnetic cavity that erupts.

One of the eruptions occurs on 2000 February 26 and involves a filament that lies along a quiet-Sun–type magnetic neutral line that extends from a nearby active region. Similarly, the second eruption, on 2002 January 4, involves a basically quiet-Sun–type filament that is located near an active region, but in this case our data are not complete enough to determine how big a role the active region plays in the eruption. We have both *Solar and Heliospheric Observatory* (*SOHO*) and *Yohkoh* data for the 2000 February eruption, but only *SOHO* data for the second event, since *Yohkoh* ceased operations in 2001 December. We first describe the morphology and dynamics of the cavity eruptions, and then discuss the implications of our observations for two proposed magnetic reconnection–based eruption models.

2. INSTRUMENTATION AND DATA

Our primary data source is *SOHO* EIT 195 Å Fe xii images at a time cadence of ~12 minutes and a spatial pixel resolution of 2.″6. EIT's full-disk coverage with uninterrupted observing periods makes it a powerful instrument for observing filament eruptions, especially slower moving ones typically associated with quiet regions. Delaboudiniere et al. (1995) give a complete description of EIT.

For the earlier event we also use data from the soft X-ray telescope (SXT), hard X-ray telescope (HXT), and the Bragg

Crystal Spectrometer (BCS) instruments on *Yohkoh*. SXT uses analysis filters spanning the approximate wavelength range 3–45 Å, effectively detecting coronal plasmas at temperatures $\gtrsim$2–3 MK. It takes either full-disk images with a pixel resolution of 9.″8 or 4.″9, or "partial frame" images that have a limited field of view but with resolution reaching 2.″5 pixels. Here we use the full-disk images, with varying time resolution from ~2 minutes to ~1 hr during times of spacecraft night or data gaps. Tsuneta et al. (1991) give SXT details. HXT data allow the synthesis of images with ~0.5 s resolution in four energy bands: 13.9–22.7, 22.7–32.7, 32.7–52.7, and 52.7–92.8 keV, which are respectively called the L, M1, M2, and H bands, as Kosugi et al. (1991) detail.

BCS generates high-resolution spectra in four narrow bandpass channels, but here we restrict our analysis to the Ca XIX channel that covers the resonance line and the associated satellite lines of He-like calcium, roughly 3.16–3.19 Å. Culhane et al. (1991) give details of the instrument. We use the spectra to determine electron temperatures during the flare associated with the 2000 February 26 eruption via the analysis method and parameters described in Sterling et al. (1997). As is typical for near-limb flares (e.g., Doschek 1990; Mariska 1994), spectra for this event were relatively symmetric and therefore a single-component fit sufficed for our analysis.

Our first eruption produced a soft X-ray *GOES* M1-class flare, with the intensity peaking around 23:40 UT on 2000 February 26, and it generated a prominent CME visible in the *SOHO* LASCO C2 coronagraph early on February 27. Our second eruption was weaker than the first in soft X-rays, producing only a *GOES* mid-C–class flare at most and peaking around 10:00 UT on 2002 January 4, but nonetheless produced a CME that first appeared in the LASCO C2 coronagraph between 09:30 and 09:54 UT on January 4. Both events occurred near the northeast solar limb.

3. OBSERVATIONS

3.1. *Event of 2000 February 26*

We examine the filament eruption of 2000 February 26, first considering its morphology and then the dynamics implied by the time-varying morphology.

3.1.1. *Morphology*

Figure 1 shows EIT 195 Å images from four times. In addition to the cool absorbing filament on the disk, which we refer to as the filament, there is also a cool feature (filament or prominence material) apparently at a higher altitude, which we refer to as a suspended feature. Extending to still higher altitudes are coronal loops, a particularly bright one of which we point out with arrows in the figure. Figures 1*a*–1*c* show the evolution of these features in time, with the coronal loop growing in size in each successive panel and the filament and suspended feature clearly moving outward between Figures 1*b* and 1*c* at least. By Figure 1*d*, the coronal loop has evolved into an "open" field, the filament is being ejected, and the suspended feature is no longer identifiable.

Figure 2 shows the same event in AlMg filter SXT images; as expected, the cool filament and suspended feature are not visible. There are, however, bright pre-eruption features in the neighborhood of the filament location, and at least three lobes (indicated by arrows in Fig. 2*a*), which are probably arcades of loops, with a larger loop enveloping the whole system (indicated by unlabeled arrows in all panels). This enveloping loop seems to be part of the same system of loops as the coronal loop visible in the EIT images. In soft X-rays also, we can see the expansion of this loop in Figures 1*a*–1*c*, while it again appears as an open field posteruption in Figure 1*d*. Figure 2*c* shows flare brightenings beginning along the location where the filament existed, but at this time the erupting lobe and the overlying coronal loop still appear to be not fully opened. Figure 2*c* also shows that at this time the middle lobe has become brighter, especially its top, and has changed morphologically, displaying a cusplike shape at the top, compared with the two images before the eruption (Figs. 2*a* and 2*b*); this middle lobe undergoes further morphological changes, including becoming more extensive, by the time of the posteruption image of Figure 2*d*. Figure 2*d* also shows strong postflare loops above the location near where the filament existed. In that same posteruption image, the rightmost lobe has also brightened and the lower corona in the region between the leftmost and rightmost lobes appears to be filled with emitting material that is either along open field lines or diffuse, while much of the higher corona above the entire region appears to contain much more material emitting along open fields than in earlier panels; thus, the region has undergone a complete morphological transformation because of the eruption.

Figure 3 shows overlays of various imaging data. Figure 3*d* shows the EIT image of Figure 3*a* overlaid on the SXT image of Figure 3*b*. Also overlaid is a hard X-ray image from the HXT L channel integrated for 16.5 s from 23:38:51 UT on 2000 February 26. Figures 3*e* and 3*f* show contours of a *SOHO* MDI magnetogram overlaid on the same EIT and SXT images, respectively.

Magnetically, Figure 3*e* shows that the region is quadrupolar, having three parallel neutral lines, with the filament tracing the southernmost one, the one bracketed by negative and positive regions southeast and northwest of the filament, respectively. Farther northwest is another negative region, and still farther northwest is another positive region. In soft X-rays the three lobes pointed out in Figure 2*a* each straddle a different one of the three neutral lines (Fig. 3*b* shows the three lobes and Fig. 3*f* shows them on the magnetic field). Finally, as we expect with cool, prominence-like material in the corona, the suspended feature in extreme-ultraviolet (EUV), pointed out in Figures 1 and 3*c*, also sits over a neutral line. Yet its neutral line is not the same as that of the filament, but rather the next neutral line northwest of the filament's neutral line; this suspended feature seems to be situated between the left and middle lobes or above the middle lobe. Figure 6*a* below shows a simplified schematic interpretation of these observations, where the suspended feature is in the dip above the magnetic null of the quadrupole, and the interior of the southern lobe of the quadruple is the magnetic cavity around the filament. In Figure 1, compared with the filament, the suspended feature appears to have a much shorter extent along the direction of the neutral lines. This is what we would expect in a three-dimensional extension of Figure 6, because the three lobes billow out on both sides of the two-dimensional plane of the center cross section shown, producing a comparatively short extent of the magnetic dip and hence a correspondingly short extent of the suspended feature. From Figures 3*d*, 3*e*, and 3*f* there is a significant hard X-ray source near the southern base of the filament, and comparison with Figures 2*c* and 2*d* shows this to be near the location of the footpoints of the soft X-ray postflare loops.

3.1.2. *Dynamics and Timings*

Next we examine the development of the filament and other cavity features around the time of the start of eruption. Figure 4

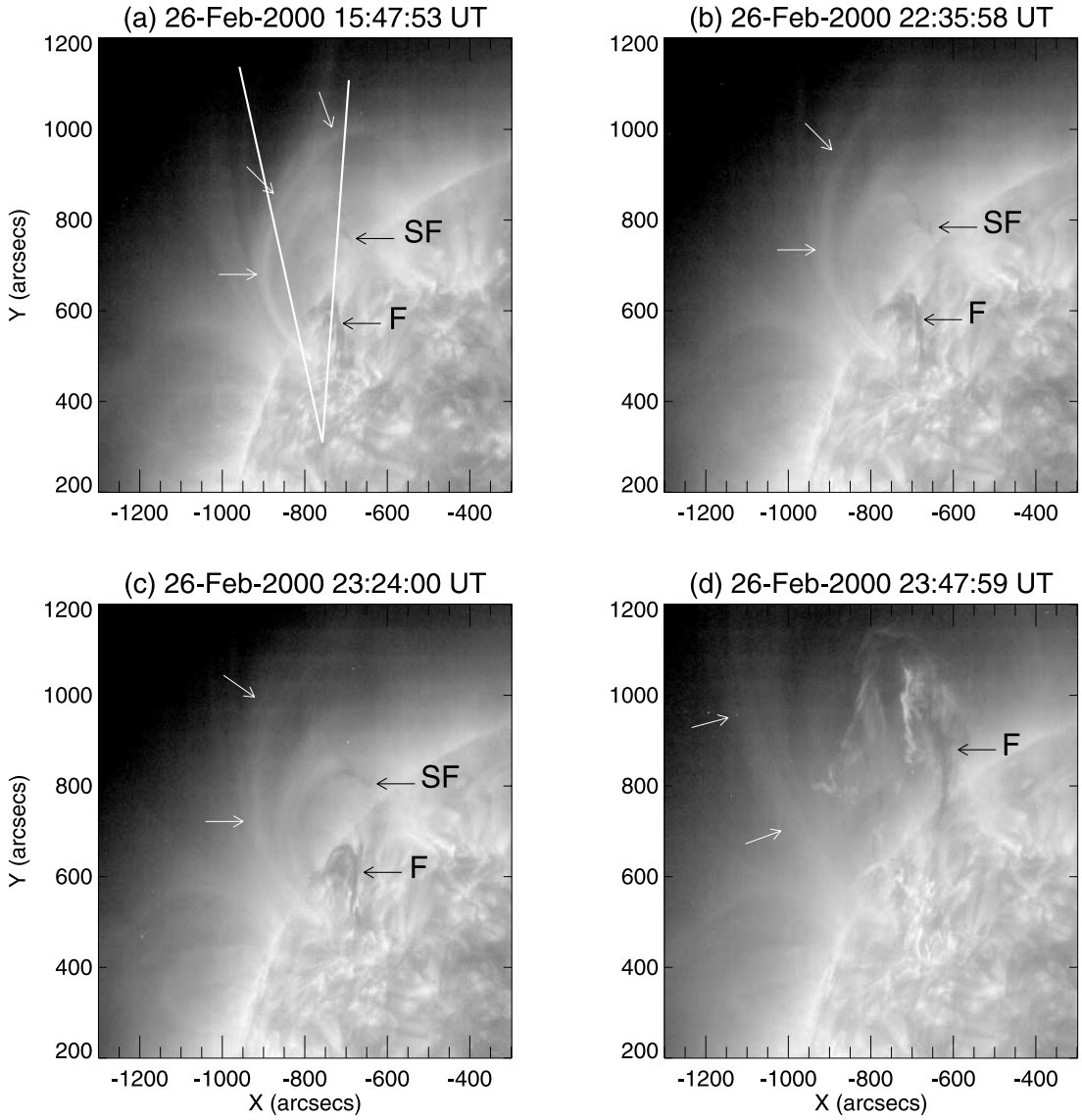

FIG. 1.—EIT 195 Å images of the 2000 February 26 filament eruption. Panels (*a*)–(*c*) show the pre-eruption phase and panel (*d*) shows the eruption underway. The labels F and SF refer to the primary filament and a filament-like suspended feature, respectively. White arrows indicate a coronal loop whose development we can follow in time; it appears as a closed but expanding loop in (*a*)–(*c*) and as an "open" field structure in (*d*). North is up and west is to the right in these and other solar images in this paper. Fiducial lines in (*a*) are used to measure the distances moved by the various features and plotted in Fig. 4. [*See the electronic edition of the Journal for a color version of this figure.*]

plots the trajectories along the fiducials of Figure 1*a* of the filament, suspended feature, and coronal loop as functions of time. In all cases the measured "heights" are with respect to the bottom of the fiducials and ignore projection effects, and therefore the numerical values for the heights are essentially arbitrary.

From 18:00 UT on 2000 February 26 for the suspended feature, and from earlier times for the filament and coronal loop, we measure a systematic rise in height for all three features. We are not confident, however, that the motions prior to 23:00 UT are real, perhaps being an artificial result of solar rotation of these near-limb features. Between 22:59:58 UT and 23:24:00 UT, however, we detect a real increase in the height of the filament, suspended feature, and probably the coronal loop with time; bearing in mind that we ignore projection effects in measuring the heights, Table 1 lists our resulting velocities. For the filament at least, this slow rise is similar to that we saw in our earlier studies of filament eruptions (Sterling & Moore 2003, 2004), as we discuss further in § 6. All three features show substantial acceleration between 23:24:00 UT and 23:35:59 UT, which we take to be the eruption onset. The similarity in the slow rise of the filament and the suspended feature, and perhaps for the coronal loop, and the closeness of the eruption onset of all three support our view that they are part of the same magnetic structure, viz., a magnetic cavity. Figure 4 also plots the hard X-ray flux from the HXT L channel as a function of time; the ramp-up starts during the 12 minute interval over which eruption onset occurs, and the peak occurs when the eruption is clearly underway.

Figure 5*a* shows the hard X-ray light curves in more detail, including fluxes from the HXT L channel and data from the *Compton Gamma Ray Observatory* (*CGRO*) BATSE channel 1 (25–50 keV) and channel 2 (50–100 keV) detectors. This is a log plot, and it shows a gradual, nearly linear (in the log) increase in the HXT L channel flux until a change in slope

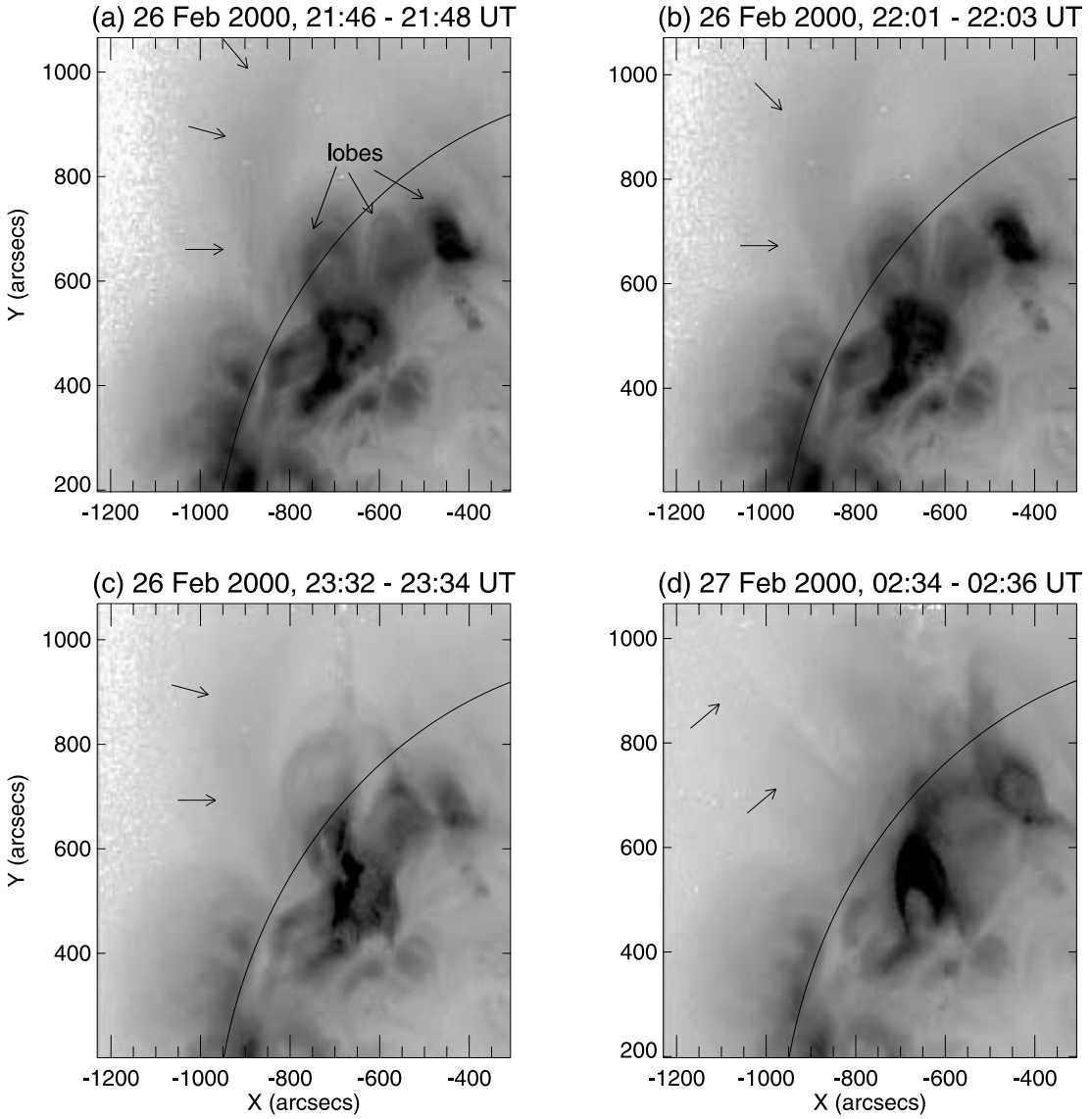

FIG. 2.—SXT AlMg negative images of the 2000 February 26 eruption from (*a* and *b*) prior to, (*c*) during, and (*d*) after the eruption. Each image is a composite of a long- and short-exposure image taken at the earlier and later times in the labels, respectively. Three soft X-ray lobes (marked in *a*) are visible before, during, and after the eruption, but the middle lobe is less apparent in (*d*), after the eruption. Unlabeled arrows in each panel show an expanding soft X-ray loop in (*a*)–(*c*), which becomes an open structure in (*d*); this feature traces the EUV coronal loop of Fig. 1. A vertical feature in (*c*) extending upward from the bright flaring core is an imaging artifact; it results from "bleeding" created by imaging the core, which is saturated in the long-exposure image.

near 23:35:40 UT. BATSE data, especially from channel 2, remain flat near background level until ~23:36:20 UT. It could be that much of the increases in flux in the softer HXT L and BATSE channel 1 plots prior to 23:36:20 UT are due to the high-energy tail of thermal X-ray emission (from flare-heated plasma) in the hard X-ray wave bands, and that significant nonthermal hard X-ray production from electron bombardment at the footpoints of flaring loops only begins with the increase of the BATSE channel 2 flux at 23:36:20 UT.

Figure 5*b* shows electron temperatures, T_e, from BCS Ca XIX spectra. Spectra prior to 23:34 UT are not reliable because of contamination of the spectra from bright active regions elsewhere on the Sun. Between 23:34:34 UT and 23:35:49 UT there is an increase in T_e, clearly indicating heating of soft X-ray–emitting plasma prior to the start of the main hard X-ray burst. There is an additional increase in T_e near the start of the first hard X-ray flux increase, and another increase starting with the second group of hard X-ray bursts beginning near 23:38 UT. This indicates that plasma heating is closely associated with the details of the hard X-ray profile; Sterling et al. (1997) saw the same trend in several flares.

Figure 6 schematically summarizes our interpretation of this event's evolution. From the initial setup in (Fig. 6*a*), the filament-carrying left lobe expands (Fig. 6*b*), and "internal" (internal to the erupting lobe) reconnection in the core of that lobe (Fig. 6*c*) occurs near the time of (and perhaps initiates) the eruption onset. "External" (external to the erupting lobe) reconnection between the left and right lobes (at the magnetic null above the middle lobe) adds new hot loops to the middle lobe (Figs. 6*c* and 6*d*), erodes the right lobe, and perhaps results in its eruption (Fig. 6*d*, although our data are not complete enough to allow us to say whether the right lobe actually erupts or just becomes activated and heated). When the filament and left lobe fully erupt (Fig. 6*e*), a CME results and the fields above the region are largely opened, as in Fig. 2*d*. After

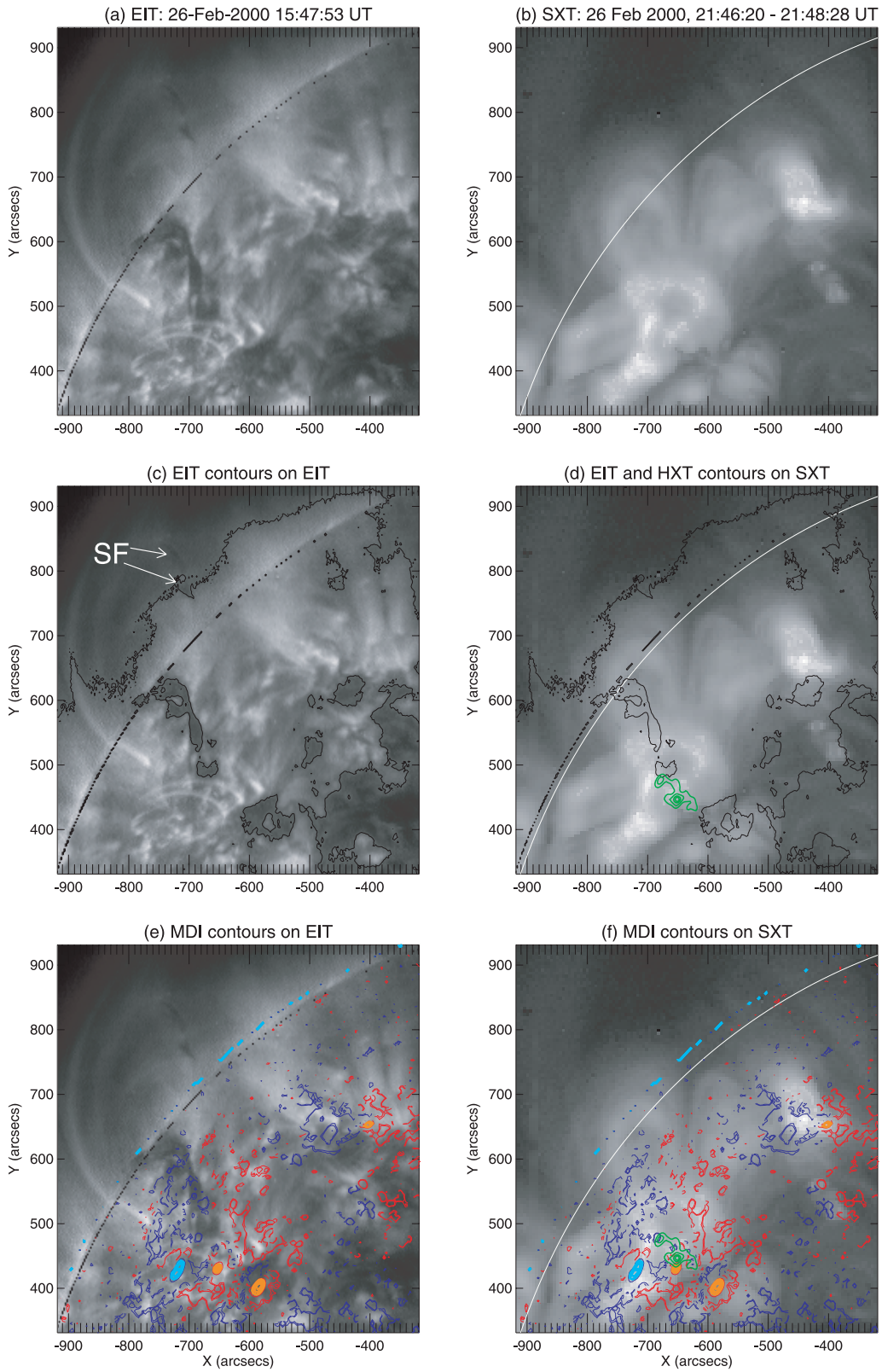

FIG. 3.—EIT 195 Å gray-scale image from 2000 February 26, 15:47:53 UT (*a*, *c*, and *e*), and SXT AlMg gray-scale image where the label times are as discussed in Fig. 2 (*b*, *d*, and *f*). In (*c*) the EIT image is contoured at the 9% level to pick out the filament, and this contour is overlaid on the SXT image in (*d*). In (*c*), SF indicates the suspended feature of Fig. 1. Green contours in (*d*) and (*f*) are HXT L channel images contoured at 10%, 25%, 50%, and 75% of the maximum value for an image integrated for 16.5 s from 23:38:51 UT on February 26, which is near the time of peak hard X-ray intensity. Blue and red in (*e*) and (*f*) are, respectively, negative and positive polarities for an MDI magnetogram from 2000 February 26 at 20:48:02 UT and contoured for values of 25, 40, and 300 G, and light blue and orange fields, also for negative and positive, respectively, are 500, 750, and 1000 G; these stronger values show one negative and three positive spots in the region (with the weakest spot near coordinates −400, 650). Magnetic field values near the limb are spurious. All images are differentially rotated to the time of the SXT images at 21:46:20 UT.

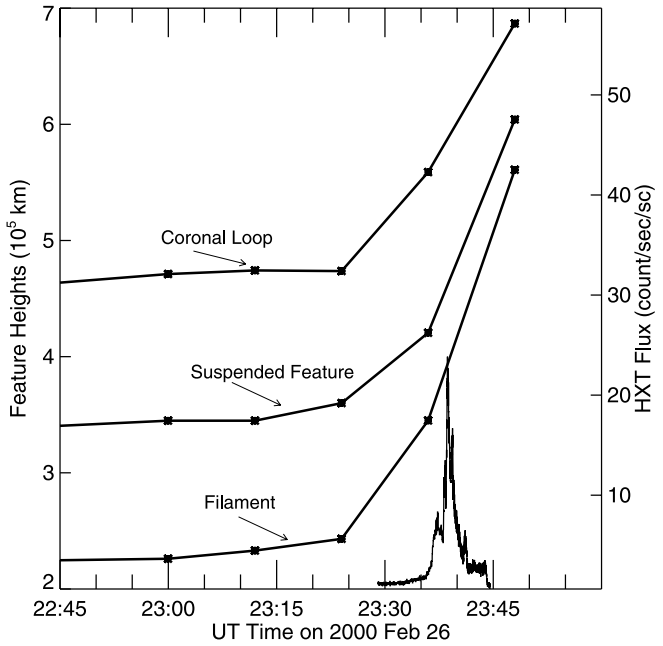

FIG. 4.—Trajectories as functions of height (with scale on left) of the filament, suspended feature, and coronal loop identified in the EIT images of Fig. 1 for the 2000 February 26 eruption, where the first two are measured along the fiducial on the right in Fig. 1*a* and the coronal loop trajectory is measured along the fiducial on the left in the same figure. Hard X-ray flux from the HXT L channel is plotted from 23:29 UT, with the scale on the right.

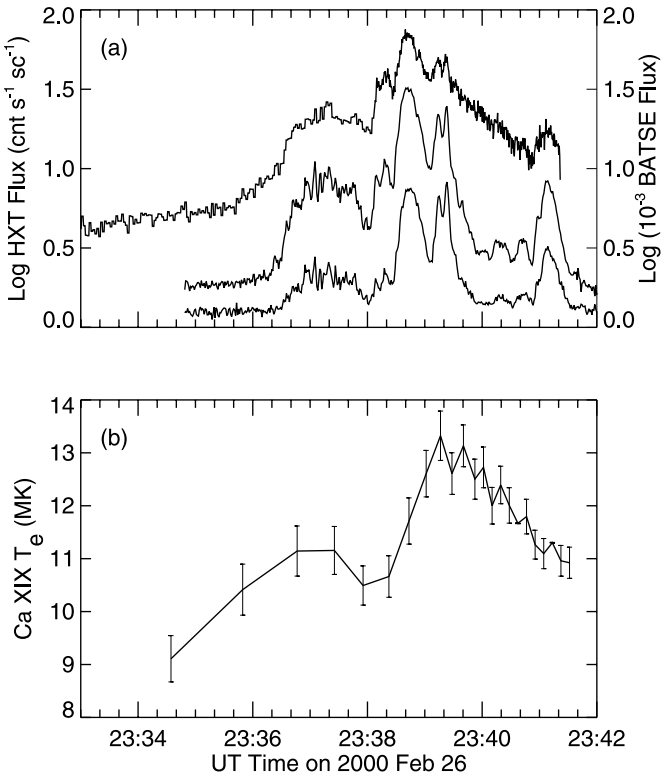

FIG. 5.—(*a*) Hard X-ray fluxes as functions of time from the HXT L (13.9–22.7 keV; *top curve*), and from the 25–50 keV (*middle curve*) and 50–100 keV (*bottom curve*) channels of BATSE on *CGRO*. For clarity, the upper (HXT) flux is shifted upward by 0.5 units (i.e., the numerical value near 23:33 UT is near 0.1) and the middle and lower curves are shifted upward by 0.27 and 0.1 units, respectively. Units of BATSE flux are counts s^{-1} 2000 cm^{-2}. (*b*) Electron temperatures derived from Ca XIX spectra from the *Yohkoh* BCS instrument. Error bars indicate 1 σ values determined from Poisson statistics of the flux count rate.

some time, we expect that the system returns to a situation nearly identical to the initial state (Fig. 6*f*′).

3.2. *Event of 2002 January 4*

3.2.1. *Morphology*

A similar filament eruption occurred on 2002 January 4, again near the east limb and again with a bright coronal loop initially residing above the filament. Figures 7*a*–7*c* show both the filament and coronal loop moving outward, with the loop apparently still closed in Figure 7*c*. In Figure 7*d*, however, the loop has "opened" in the sense that it appears to have extended out to several solar radii, with the loop legs showing little curvature over the field of view of the image. In this image the filament appears in emission as it leaves the Sun, and bright flare ribbons are visible in the filament channel.

An MDI magnetogram (Fig. 7*b*) shows that the magnetic configuration for this event is similar to the 2000 February 26 event in that it is quadrupolar, but there is no strong field at the end of the erupting filament, in contrast to the previous case. This time the filament lies along the middle of three neutral lines of the quadrupole. We see no indication of cool suspended features high above any of the neutral lines in the EIT 195 Å images, in contrast to the previous case, nor did we see any such features in EIT 284 Å Fe XV images taken on the day of the eruption. Another difference from the previous case is that the visible coronal loop appears to be part of the middle lobe instead of overlying the entire quadrupole. The side lobes are not clearly visible in the 195 Å images here, nor in EIT 284 Å images before and after the eruption: these lobes might have been more visible in soft X-rays, as was the case with the previous event (cf. Figs. 1*a* and 2*a*). Our impressions of the pre-eruption setup, including the side lobes, are reflected in the schematic in Figure 9*a* below.

3.2.2. *Dynamics and Timings*

Figure 8 shows the trajectories of the filament and coronal loop of Figure 7 measured along the fiducial lines of Figure 7*a*. As with the previous case, absolute values for the heights are

TABLE 1

VELOCITIES OF FEATURES IN FIGURE 5

2000 February 26 Time Range (UT)	Filament Velocity[a] (km s^{-1})	Suspended Feature Velocity (km s^{-1})	Loop Velocity (km s^{-1})
22:59:58–23:24:00.....	12	10	2
23:24:00–23:35:59.....	140	85	120
23:35:59–23:47:59.....	300	250	180

[a] All velocities are in the plane of the image and are averages over the specified time ranges.

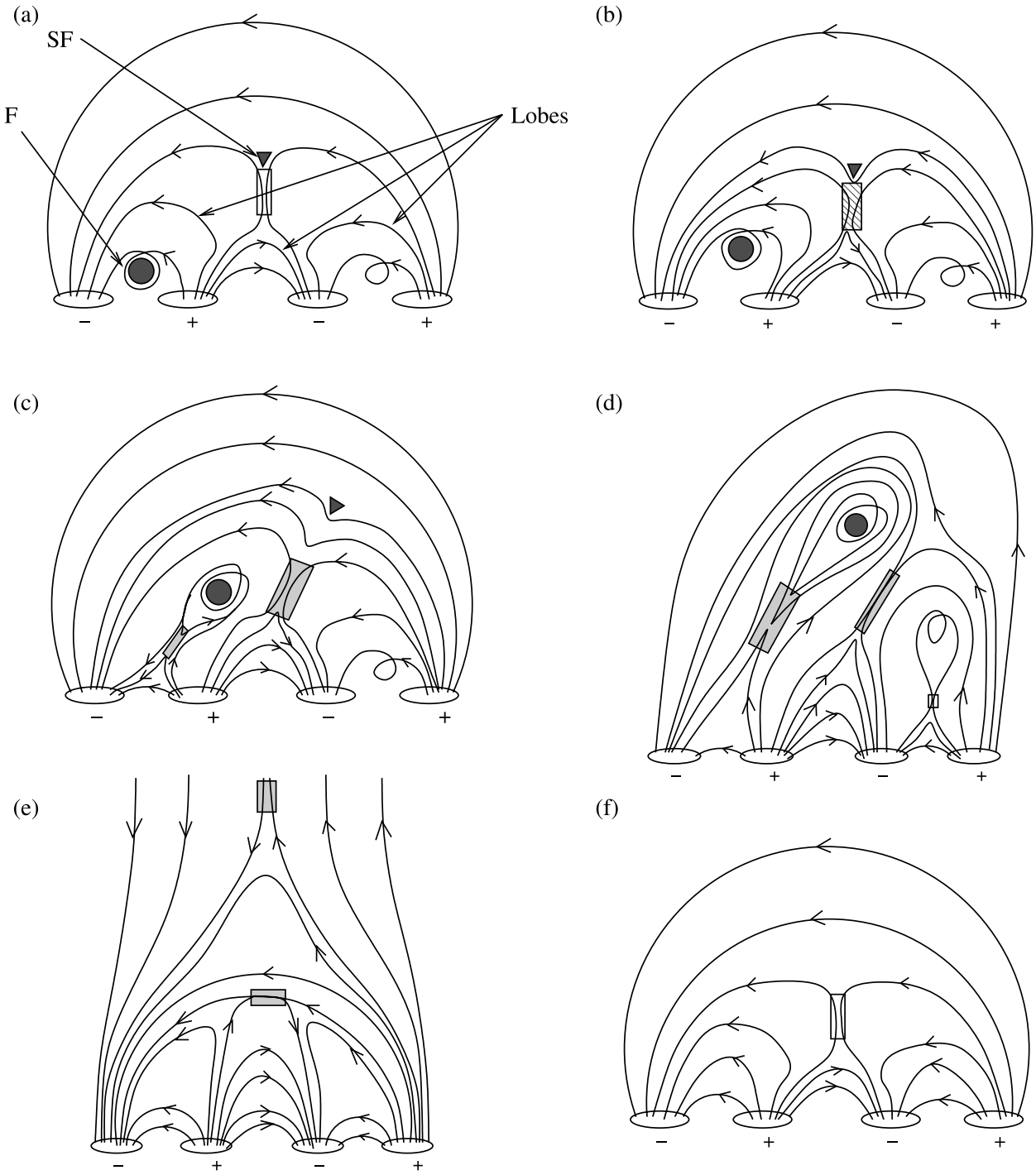

FIG. 6.—Schematic interpretation of the 2000 February 26 eruption: (*a*) Before the start of the slow rise of the left-lobe cavity; F and SF represent the filament and suspended feature of Fig. 1, respectively, and "Lobes" are as identified in Fig. 2*a*. The transparent rectangle indicates the location where reconnection can start. (*b*) During the slow rise of the left lobe; the shaded rectangle (here and in all other panels) shows locations where we expect reconnection to be occurring. (*c*) Early in the fast eruption of the left lobe. (*d*) During the activation or eruption of the right lobe; reconnection may be occurring in the transparent box in right lobe, but our observations have not confirmed this. (*e*) Late-phase reclosing of the opened quadrupole. (*f*) Approaching initial configuration of panel (*a*); the transparent rectangle indicates the location where reconnection can start.

somewhat arbitrary, being measured relative to the point at the base of the fiducials in Figure 7*a* and ignoring projection effects. For the filament at least, the rise appears smoother than in the Figure 5 case, and could be fit with a single smooth curve. Nevertheless, consistent with Table 1 we present representative velocities over a few time intervals in Table 2. Early on the filament's rise is again ~10 km s^{-1}, but it rapidly reaches speeds in excess of 50 km s^{-1}. Similarly, the coronal loop begins with about a 10 km s^{-1} rise before rapidly erupting upward; its trajectory appears to be less smooth than that of the filament, but the sampling is too poor to draw strong conclusions about this. Both the filament and the coronal loop undergo a clear slow-rise phase between ~08:00 UT and 09:00 UT, with both erupting between 09:00 UT and 09:12 UT.

As with the 2000 February 26 eruption, the close tracking of movement between the filament and the coronal loop

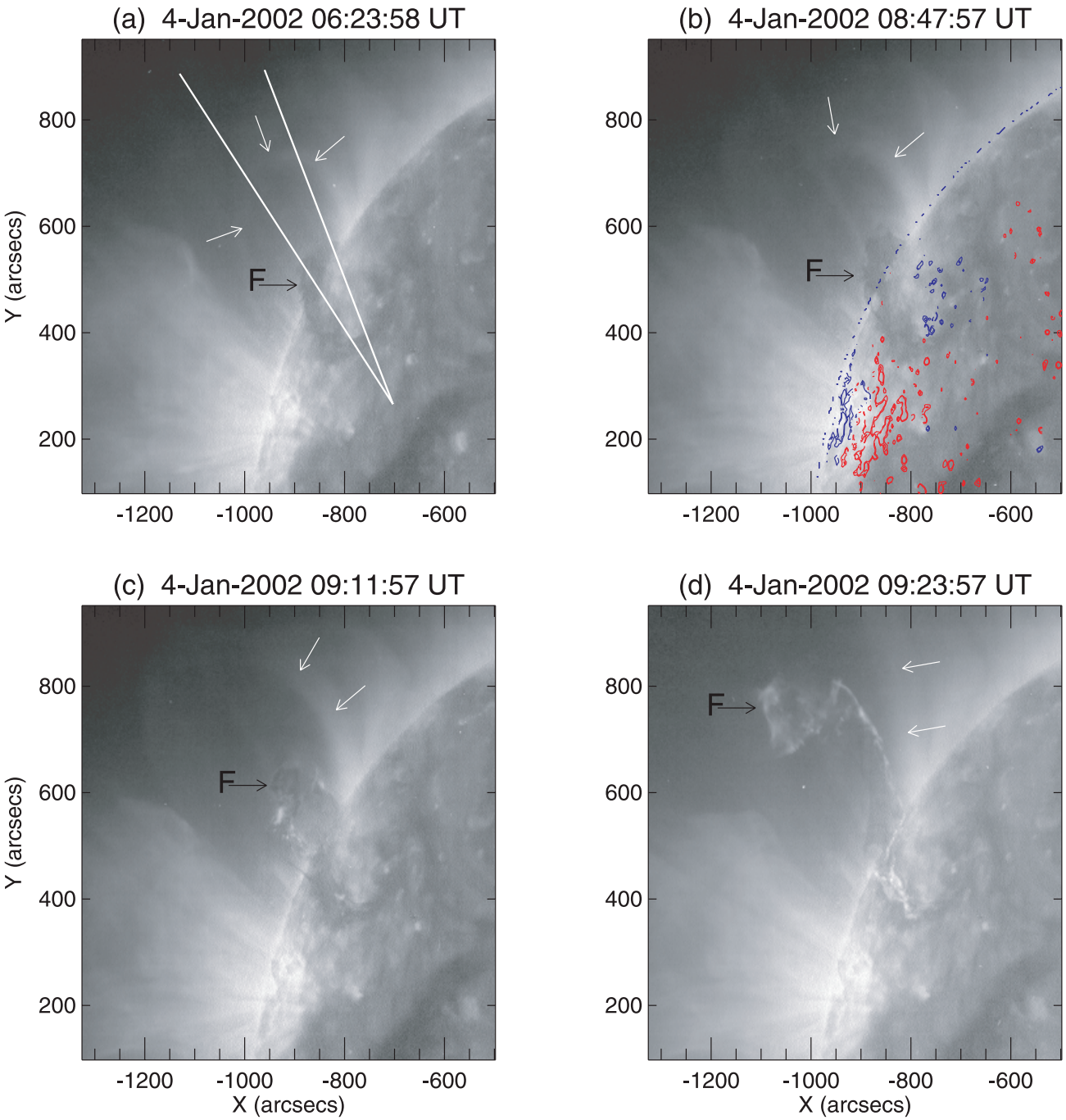

FIG. 7.—EIT 195 Å images of the 2002 January 4 filament eruption. Panels (*a*)–(*c*) show the pre-eruption phase and panel (*d*) shows the eruption underway. Label F refers to the filament and unlabeled white arrows indicate a coronal loop whose development we can follow in time. As in Fig. 1, in this case also the loop appears as closed but expanding in (*a*)–(*c*) and as an open field structure in (*d*). Fiducial lines in (*a*) are used to measure the distances moved by the various features and are plotted in Fig. 8 below. Blue and red in (*b*) are contours from an MDI magnetogram at 2002 January 4 12:51:00 UT, where values and contour levels are as described in Fig. 3; all values are <500 G, and values at the limb are spurious.

indicates that they belong to a common magnetic cavity. In this case a correlation between the filament and the loop in the pre-eruption period is more apparent than in the previous example, and this may be a consequence of a longer pre-eruption slow-rise phase in this case. Alternatively, it could be due to this loop being more directly related to the erupting lobe than the loop in the previous case; specifically, it may be a part of the center lobe, while the loop in the 2000 February 26 event may have been overlying (external to) all three lobes of that event.

Figure 9 schematically summarizes our interpretation of this event's evolution. From the initial setup (Fig. 9*a*), the middle lobe and filament undergo a slow rise, leading to external reconnection between the middle lobe and overlying fields (Fig. 9*b*). At some point this expansion speeds up as eruption onset takes place (Fig. 9*c*), with internal reconnection beneath the filament starting. Following this the middle lobe and filament are ejected (Fig. 9*d*), with the entire cavity opening up in the higher corona, similar to Figure 6*e* for the previous case. At later times we expect reconnection to continue in the

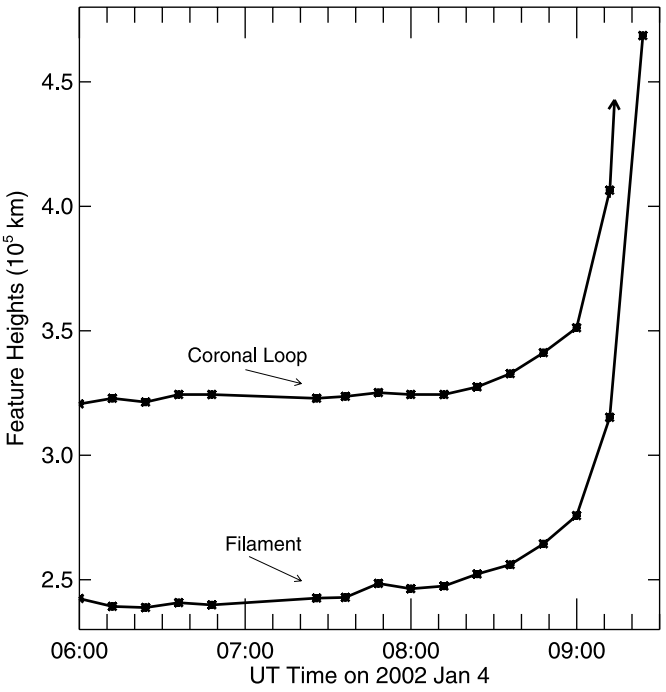

FIG. 8.—Trajectories as functions of height (with scale on left) of the 2002 January 4 filament and coronal loop identified in the EIT images of Fig. 7, where the filament is measured along the fiducial on the left in Fig. 7*a* and the coronal loop trajectory is measured along the fiducial on the right in the same figure; at the last time value (09:23:57 UT), the coronal loop is out of the field of view.

corona until a state similar to that prior to eruption (Fig. 9*a*) again ensues. Obviously, this schematic picture is more speculative than for the 2000 February 26 case because of the absence of *Yohkoh* data.

4. CAVITY AND FILAMENT MASS CONTENT

We can estimate the mass of material in the magnetic regions, or magnetic cavities, for our two events; in both cases we will compare with the masses of the respective filaments. First we consider the 2000 February 26 case. For the filament, from Figure 1*a* the width is $\sim 3 \times 10^4$ km and from Figure 1*d* the extent of the erupting filament might be $\sim 2.5 \times 10^5$ km. If we take it to be cylindrical and have a filling factor of 10%, and to have a density of 10^{10}–10^{11} cm^{-3} as is typically quoted for filaments (e.g., Schmahl & Hildner 1977; Rust et al. 1980), we obtain a mass $M \sim 10^{14}$–10^{15} g, which is the same as Sterling & Moore (2003) found for a prominence. For the cavity, we first estimate its size based on the height of the suspended feature, which from Figure 1*a* is roughly 2×10^5 km. Taking the cavity to be a cylinder of this width and having length equal to that of the filament, and using a coronal density of 10^8–10^9 cm^{-3}, which is an approximate value for average quiet-Sun features (e.g., Priest 1982), we obtain a coronal cavity mass of $M \sim 10^{15}$–10^{16} g. This means that the mass of the cavity is comparable to or up to 2 orders of magnitude larger than that of the filament alone. If instead the cavity densities are similar to those of coronal holes (a few $\times 10^7$ cm^{-3}; e.g., Doschek et al. 1997) then the cavity mass could be comparable to that of the filament.

For the 2002 January 4 filament the coronal loop's motion closely mimics the filament's trajectory, and so we assume both to be part of the same cavity. From Figure 7, the filament appears to have dimensions similar to the filament in Figure 1, and the height of the coronal loop in Figure 7 is also similar to the height of the suspended feature in Figure 1. Therefore, the mass values are about the same for both of our filaments and cavities.

TABLE 2

VELOCITIES OF FEATURES IN FIGURE 7

2002 January 4 Time Range (UT)	Filament Velocity[a] (km s^{-1})	Loop Velocity (km s^{-1})
08:23:57– 08:59:57	10	10
08:59:57– 09:11:57	55	75
09:11:57– 09:23:57	215	...

[a] All velocities are in the plane of the image and are averages over the specified time ranges.

For CMEs with the three-part structure discussed in § 1, values for the total CME mass are quoted as 10^{15}–10^{16} g, where the filament material alone makes up only ~10% of this total (e.g., Kahler 1992). This fits with our cavity and filament mass estimates if the material and magnetic field in and around the erupting cavity become the CME. Also, our observations could address a "missing mass" issue regarding SXT observations of CME source regions: for four CMEs, Sterling & Hudson (1997) and Hudson et al. (1998) found that the soft X-ray dimmings from the source regions of the CMEs added up to masses of only $\sim 10^{14}$ g, which is an order of magnitude or more lower than that of typical CMEs. If most of the cavity material is of low temperature (1–2 MK) then much of it would not show up in SXT images, so only a small fraction of the material, perhaps an amount comparable to that of the filament, may be all that is bright enough to enter the mass calculation based on SXT images. Hudson et al. (1999) found temperatures for their cavity to be between 1.5 and 2.0 MK, which is near the lower limit for detectability with SXT. Material near these temperatures could be more prominent in EUV, and in fact mass measurements based on CME source region dimmings in EIT images by Wang et al. (2002) and Harrison et al. (2003) do give masses close to those measured in CMEs. Gopalswamy & Hanaoka (1998) estimated the mass of the cavity they observed to be $\sim 10^{15}$ g based on dimmings in SXT images, an order of magnitude higher than the SXT results of Sterling & Hudson (1997) and Hudson et al. (1998). This higher value could be due to the Gopalswamy & Hanaoka (1998) event occurring over the limb, while the Sterling & Hudson (1997) and Hudson et al. (1998) events were all on the disk; that is, for some reason subtle posteruption SXT dimmings might be more apparent against an above-the-limb coronal background than against a solar disk background. Another possibility is that the Gopalswamy & Hanaoka (1998) event was particularly large.

5. ERUPTION MECHANISM

We consider the implications of our observations for two specific eruption mechanism suggestions, the "tether-cutting" model and the "breakout" model.

5.1. *Tether Cutting*

This idea, put forth and developed by Moore & Labonte (1980), Sturrock (1989), Moore & Roumeliotis (1992), and Moore et al. (2001), holds that the key release mechanism for eruptions involves a single highly sheared magnetic bipole. Reconnection (internal reconnection in the terminology of our descriptions of Figs. 6 and 9) between sheared field lines in

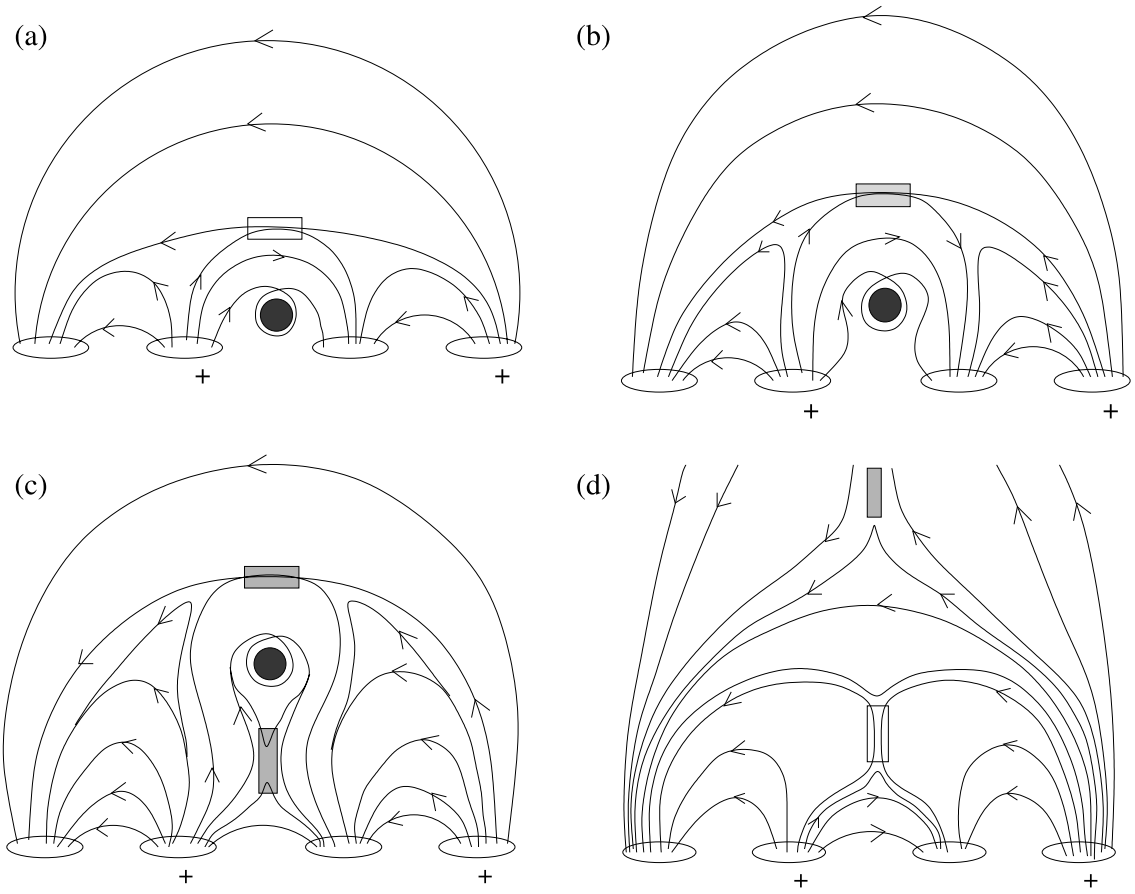

FIG. 9.—Schematic interpretation of the 2002 January 4 eruption: (*a*) Before the onset of the slow rise of the middle lobe; the transparent rectangle indicates the location where reconnection can start, and the dark shaded circle (here and in other panels) represents the erupting filament. (*b*) During the slow rise of the middle lobe; the shaded rectangle (here and in all other panels) shows locations where we expect reconnection to be occurring. (*c*) Early in the fast eruption of the middle lobe. (*d*) Late-phase reclosing of opened quadrupole; the transparent rectangle indicates the location where reconnection may still be occurring. Eventually the system closes down to resume a state similar to that in (*a*).

the core of the bipole cuts magnetic field lines (''tethers'') that tie down the core magnetic field, coronal material, and filament (if present), unleashing the sheared core field to erupt. Filaments often begin their upward movement slowly and then undergo rapid acceleration, as in the two cases here (Figs. 4 and 7) and elsewhere (e.g., Tandberg-Hanssen et al. 1980; Kahler et al. 1988; Sterling & Moore 2003, 2004). In tether cutting, the idea is that the initial slow-rise phase might be caused by any number of factors, such as emerging flux or reconnection in the core (in which case it could be photospherically driven ''nonrunaway'' tether cutting, of the type discussed by Moore & Roumeliotis 1992; Chen & Shibata 2000 and Lin et al. 2001 present numerical simulations of the basic processes involved) or reconnection elsewhere, but the onset of the rapid upward movement only occurs when rapid (''runaway'') tether-cutting reconnection begins in the core.

A signature of this runaway reconnection can be soft X-ray brightening in the sheared core field, as found by Moore et al. (2001). Such brightening around the time of the start of the fast filament rise would be consistent with tether cutting. We can check this idea with the 2000 February 26 event. Our SXT image in Figure 2*c* shows that soft X-ray brightening exists in the core region by 23:32 UT; we have found that this brightening exists since at least 23:27:28 UT in an SXT Al.1 filter image, and this is the earliest appropriate image available during that *Yohkoh* orbit for investigating this question. Since the filament fast rise begins between 23:24 UT and 23:36 UT (Fig. 4; Table 1), the SXT observations are consistent with tether cutting initiating the fast-eruption onset. Moreover, Sterling & Moore (2003) point out that a detectable level of soft X-rays from tether cutting could be delayed relative to fast-eruption onset in the case of weak eruptions, although it appears as if the delay is not more than a few minutes at most in the present case.

Another possible signature of tether cutting is enhanced hard X-ray flux, when enough high-energy electrons reach the low atmosphere along the reconnecting field lines. Checking this with the 2000 February 26 event, Figures 4 and 5*a* show that the hard X-ray rate increases from 23:35:40 UT in the softest channel (HXT L) and from 23:36:10 UT in our hardest channel (BATSE channel 2). This suggests that the fast eruption begins between ~11 minutes before and ~20 s after the HXT L hard X-ray onset, and the early acceleration would have to have been very large to reach the observed heights within 20 s. This suggests that the onset of the fast eruption most likely began some minutes prior to the upturn in hard X-ray flux. Therefore, if tether cutting initiates the fast eruption it must be at such a level as to result in the onset of fast filament eruption prior to producing detectable hard X-rays at energies above ~25 keV.

Figure 5*b* shows an increase in the soft X-ray temperature of the flaring plasmas, indicating increased plasma heating, prior to the onset of substantial hard X-rays. This heating could be due to reconnection-related heating, including an

increase in the high-temperature plasma emission measure due to the evaporation of newly heated plasmas from incipient flare loops. Inspection of spectra from prior to the first plotted datum suggests the presence of even earlier pre-eruption heated plasma, but the background from nearby active regions contaminates the earliest spectra (which are of very low intensity) and so we are unable to make definitive comments on this point for this event.

5.2. *Breakout*

A suggestion of Antiochos (1998) and Antiochos et al. (1999) holds that the fundamental magnetic configuration for eruptions is multibipolar rather than a single bipole. An example is a quadrupole configuration where a highly sheared "inner" bipole is initially trapped beneath the field of an enveloping "outer" bipole. If the two bipoles have the correct relative orientation, and if flux emergence or some other process causes the inner bipole to push upward, then reconnection (external reconnection in our terminology for Figs. 6 and 9) between the inner bipole and outer bipole fields can result in the creation of new "side lobe" coronal loops while the remaining inner bipole fields escape into the heliosphere as a CME. If the early reconnection between the inner and outer bipoles is slow enough (i.e., if the electrical conductivity remains high enough for long enough), a large stress can build up at the boundary as the slow reconnection progresses. Then, when the reconnection finally switches to being fast, the pent-up inner fields explosively break out through the field of the outer bipole and escape from the Sun. As the inner bipole fields are escaping, tether-cutting–like internal reconnection will occur among its outstretched fields reaching back to the surface, resulting in a standard solar flare. The key difference between the tether-cutting model and the breakout model is that in tether cutting internal reconnection is what allows the outward acceleration of the erupting fields, and this can occur independently of whether there are surrounding or overlying (e.g., outer bipole) fields; only the single sheared-core bipole is critical. In contrast, according to the breakout idea the fast eruption does not occur unless the overlying fields are there to assist in the stress buildup at a neutral-sheet boundary between the two flux systems. In addition to the original breakout papers, several others also show schematic diagrams of the breakout setup (e.g., Aulanier et al. 2000; Klimchuk 2001; Sterling & Moore 2004)

We now ask whether the observations of our two events are consistent with breakout. Both eruptions take place in multibipolar field configurations (Figs. 3*e*, 3*f*, and 7*b*), which is the first requirement for breakout. Moreover, Figures 2 and 3 show that there are soft X-ray coronal loops or arcades (the lobes in Fig. 2*a*) straddling the three magnetic neutral lines in the quadrupolar magnetic pattern (Fig. 3*f*). Figure 3 also shows that the suspended feature in the first event is above the middle neutral line, and so may reside above the elevated magnetic null of the quadrupole (Fig. 6*a*). Although the classic picture for breakout has the main eruption occurring in the middle of three lobes, we can imagine the same principle applying to one of the side lobes instead, and that would be the case with this 2000 February 26 event, with the eruption occurring in the southernmost of the three lobes and with the highest bright coronal loop representative of the overlying fields. (See Wang et al. 2002 for another example of suggested breakout in a nonclassic setup.) For the 2002 January 4 event, we envision a more classical breakout setup, with the erupting lobe in the middle of the quadrupole (Fig. 9*a*). We conclude that, within the limitations of our observations, our findings are consistent with breakout occurring in both events.

However, just because the basic breakout setup exists it does not necessarily follow that breakout is actually operating or that it is the primarily cause of the eruption; it could be that some other mechanism, e.g., a single-bipole mechanism similar to tether cutting, could be operating in a magnetic environment that happens to be more complex, resulting in breakout-like reconnection in the corona. We cannot address further here the question of whether the breakout-like signatures are essential to the eruption rather than secondary; however, in the future it may be possible to compare our observations with predictions from numerical simulations modeling breakout. Such comparisons might consider, for example, how much the overlying coronal loops have expanded by the time of the start of the soft X-ray and hard X-ray emissions from the core, along with the corresponding evolution of the rising filament.

6. DISCUSSION

Our observations of two filament eruptions suggest that in each case the filament resides at the base of a much larger scale coronal magnetic cavity, and that the entire cavity is involved in the eruption. Tracking the filament and features in the inferred cavities shows that both undergo an initial slow rise, followed by acceleration to higher velocities. In the 2000 February 26 case the trajectories seem to be in two distinct phases, a slow-rise and a fast-rise phase, and this is similar to two eruptions we observed earlier (Sterling & Moore 2003, 2004). Those earlier studies showed velocities of the order of 1 and 10 km s^{-1}, respectively, in their slow and fast phases, which is up to an order of magnitude lower than the velocities for our two events here. This could be due to the earlier events both occurring in isolated quiet solar regions, while both events in the current paper occur in association with nearby active regions. Another factor is that we did not account for line-of-sight projection effects in calculating velocities for either the previous two events or the current two events, and so the actual upward velocities might be closer than the quoted projected values alone indicate. As mentioned earlier, there have been other observations of slow filament rise before faster eruption. In addition, some soft X-ray features show acceleration near eruption-onset time (e.g., Ohyama & Shibata 1997; Alexander et al. 2002); such features may be related to the slow-then-fast–erupting phenomena we observe.

In considering our observations in terms of the tether-cutting and the breakout models, our 2000 February 26 event shows that the plasma heating and the increase in the soft X-ray intensity occur during the 12 minute interval over which the fast-filament eruption begins, although the time cadence of the EIT images prevents us from determining how much closer the two occurrences coincide. These data do show, however, that fast eruption begins prior to the time that the hard X-ray flux rises significantly above background level. Thus, if tether cutting is responsible for the eruption, it must allow for the fast onset prior to producing significant hard X-ray flux. This means that, as best as we can determine with these data, the tether-cutting model can be consistent with our observations, but a constraint is that at the time (within a 12 minute window) of the eruption onset there must be significant soft X-ray flux and insignificant hard X-ray flux. We do not know why the hard X-rays should not start together with the onset of fast tether-cutting reconnection; it could be that a minimum rate of reconnection is required to produce the

hard X-rays, and the earliest fast tether-cutting reconnection occurs at a rate less than that critical value. This is pure speculation, however. We can only say that, for this event at least, delayed hard X-ray emission is a constraint the tether-cutting model must satisfy if it is correct.

Our observations are qualitatively consistent with the breakout model, with both eruptions occurring in quadrupolar magnetic configurations and both showing pre-eruption expansions of elevated coronal fields. Just how the specifics of the observations fit with breakout-model predictions should be considered in future investigations and refinements of that model. Our observations place constraints on the configuration of the overlying fields at the time of the start of the filament's fast-phase onset and the relative times of onset of soft and hard X-ray emissions.

With this study we were not able to rule in or rule out either the tether-cutting model or the breakout model, but we have determined new constraints for these or any other model, albeit for only the two specific events that we examined here. Within these constraints, our observations of the 2000 February eruption (and of the 2002 January eruption also, but based on less complete data) are consistent with runaway tether-cutting–type reconnection and fast breakout–type reconnection both beginning nearly simultaneously near the start of the fast eruption, with one of these mechanisms perhaps initiating fast-eruption onset and with both being important in further unleashing the fast eruption once it has started. We have not examined other suggested eruption mechanisms, such as a magnetic instability (e.g., Rust & Kumar 1996; Sturrock et al. 2001), and so we cannot comment on whether they might more naturally fit the observations. Some recent reviews of CME eruption mechanisms are Forbes (2000), Klimchuk (2001), and Lin et al. (2003).

Our conclusions are tempered by the low cadence of our data, particularly EIT data, compared with the rates of change of the various phenomena around the time of eruption onset. For example, we only have one measurement of the 2000 February 26 filament's height near the time of the onset of the hard X-rays in Figure 4. We are also limited by our single–line-of-sight views of the eruptions; for example, the fields we see carrying the filaments, suspended feature, or coronal loops might be displaced from the fields most directly involved in the eruptions, in which case their responses could be delayed from that of the main erupting fields. For these reasons, repeated observations of similar events would be beneficial.

We thank K. Matsuzaki and D. M. Zarro for computer and software assistance, T. Kosugi for in-residence support in Japan, and L. K. Harra and T. Magara for useful discussions. Both authors were supported by funding from NASA's Office of Space Science through the Solar Physics Supporting Research and Technology Program and the Sun-Earth Connection Guest Investigator Program. *Yohkoh* is a mission of the Institute of Space and Astronautical Sciences (Japan), with participation from the US and UK, and *SOHO* is a project of international cooperation between ESA and NASA. A portion of this work was carried out while A. C. S. was employed by United Applied Technologies, Huntsville, AL.

REFERENCES

Alexander, D., Metcalf, T. R., & Nitta, N. V. 2002, Geophys. Res. Lett., 29, 41
Antiochos, S. K. 1998, ApJ, 502, L181
Antiochos, S. K., DeVore, C. R., & Klimchuk, J. A. 1999, ApJ, 510, 485
Aulanier, G., DeLuca, E. E., Antiochos, S. K., McMullen, R. A., & Golub, L. 2000, ApJ, 540, 1126
Chen, P. F., & Shibata, K. 2000, ApJ, 545, 524
Culhane, J. L., et al. 1991, Sol. Phys., 136, 89
Delaboudiniere, J.-P., et al. 1995, Sol. Phys., 162, 291
Doschek, G. A. 1990, ApJS, 73, 117
Doschek, G. A., et al. 1997, ApJ, 482, L109
Forbes, T. G. 2000, J. Geophys. Res., 105, 23153
Gopalswamy, N., & Hanaoka, Y. 1998, ApJ, 498, L179
Harrison, R. A., Bryans, P., Simnett, G. M., & Lyons, M. 2003, A&A, 400, 1071
Hudson, H. S., Acton, L. W., Harvey, K. L., & McKenzie, D. E. 1999, ApJ, 513, L83
Hudson, H. S., Lemen, J. R., St. Cyr, O. C., Sterling, A. C., & Webb, D. F. 1998, Geophys. Res. Lett., 25, 2481
Kahler, S. 1992, ARA&A, 30, 113
Kahler, S. W., Moore, R. L., Kane, S. R., & Zirin, H. 1988, Sol. Phys., 328, 824
Klimchuk, J. A. 2001, Geophys. Monogr., 125, 143
Kosugi, T., et al. 1991, Sol. Phys., 136, 17
Lin, J., Forbes, T. G., & Isenberg, P. A. 2001, J. Geophys. Res., 106, 25053
Lin, J., Soon, W., & Baliunas, S. L. 2003, NewA Rev., 47, 53
Mariska, J. T. 1994, ApJ, 434, 756
Moore, R. L., & LaBonte, B. 1980, in Solar and Interplanetary Dynamics (Dordrecht: Reidel), 207
Moore, R. L., & Roumeliotis, G. 1992, in Eruptive Solar Flares, ed. Z. Svestka, B. V. Jackson, & M. E. Machado (Berlin: Springer), 69
Moore, R. L., Sterling, A. C., Hudson, H. S., & Lemen, J. R. 2001, ApJ, 552, 833
Ohyama, M., & Shibata, K. 1997, PASJ, 49, 249
Priest, E. R. 1982, Solar Magnetohydrodynamics (Dordrecht: Reidel)
Rust, D. M., & Kumar, A. 1996, ApJ, 464, L199
Rust, D. M., et al. 1980, in Skylab Solar Workshop II: Solar Flares (Boulder: Colorado Assoc. Univ. Press), 273
Schmahl, E., & Hildner, E. 1977, Sol. Phys., 55, 473
Sterling, A. C., & Hudson, H. S. 1997, ApJ, 491, L55
Sterling, A. C., Hudson, H. S., Lemen, J. R., & Zarro, D. A. 1997, ApJS, 110, 115
Sterling, A. C., & Moore, R. L. 2003, ApJ, 599, 1418
———. 2004, ApJ, 602, 1024
Sturrock, P. A. 1989, Sol. Phys., 121, 387
Sturrock, P. A., Weber, M., Wheatland, M. S., & Wolfson, R. 2001, ApJ, 548, 492
Tandberg-Hanssen, E., Martin, S. F., & Hansen, R. T. 1980, Sol. Phys., 65, 357
Tsuneta, S., et al. 1991, Sol. Phys., 136, 37
Wang, T., Yan, Y., Wang, J., Kurokawa, H., & Shibata, K. 2002, ApJ, 572, 580